

# Passive Magnetic Attitude Control for CubeSat Spacecraft

David T. Gerhardt

*University of Colorado, Boulder, CO 80309*

Scott E. Palo

*Advisor, University of Colorado, Boulder, CO 80309*

The National Science Foundation has begun funding CubeSats for space weather investigation. Many of these missions are to measure charged particles in a highly inclined Low Earth Orbit (LEO). The charged particles spiral around magnetic field lines as they reach LEO. Passive Magnetic Attitude Control (PMAC) aligns a CubeSat to within  $\pm 15^\circ$  of the Earth's local magnetic field line throughout each orbit, maximizing particle counts available for onboard science instrumentation. Also, given typical CubeSat mass ( $< 4$  kg) and power ( $< 6$ W insolated without deployable solar panels) constraints, PMAC is ideal as it performs using low mass ( $< 50$ g) and no power. The design of a PMAC system is discussed for a 3U CubeSat, considering external torques acting on the craft, parametric resonance, and apparent permeability of the hysteresis rod. Next, the development of a PMAC Matlab simulation is discussed, including equations of motion, an Earth magnetic field model, and hysteresis rod response. Key steps are outlined with sufficient detail to recreate the simulation. Finally, the simulation is used to verify the PMAC system onboard the NSF-funded Colorado Student Space Weather Experiment (CSSWE).

## Introduction

**S**OLUTIONS for satellite attitude control must be weighed by trade of resources vs. performance. CubeSats are a unique form factor varying from one (1U) to three (3U) stacked cubes of dimensions  $10 \times 10 \times 10$  cm. For these small satellites, Passive Magnetic Attitude Control (PMAC) is a robust attitude solution particularly useful for space weather investigation. PMAC is composed of a bar magnet to supply restoring torque and a hysteresis rod to supply dampening torque. As a passive system, PMAC draws no system power and, for microsattellites and smaller, uses less than 50 grams of mass. The concept was space-tested in 1960 on *Transit-1B*, and has been used moderately since then. PMAC is sometimes not a desirable solution because its pointing is typically limited to oscillations  $\pm 15^\circ$  about the local magnetic field.<sup>1</sup> However, when a mission has low resource availability and benefits from alignment with the Earth magnetic field, PMAC is a wise solution.

The National Science Foundation began funding CubeSats for space weather investigation in 2008 with Michigan's RAX CubeSat. The Michigan team chose PMAC for their CubeSat, and have developed an air-bearing testbed in lieu of modeling the system behavior.<sup>2</sup> The University of Colorado's Colorado Student Space Weather Experiment (CSSWE) has also chosen a PMAC system. Its mission involves sensing high-energy charged

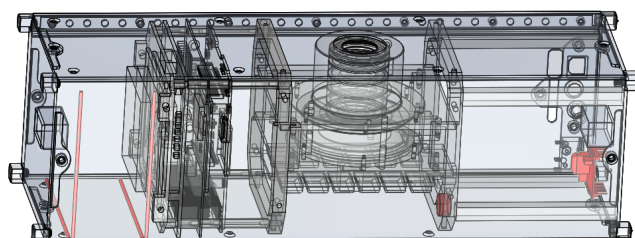


**Figure 1. CSSWE Magnetic Components.**

particles which spiral around magnetic field lines. Aligning with the local magnetic field maximizes the particles available for the CSSWE science instrument: the Relativistic Electron Particle Telescope integrated little experiment (REPTile).<sup>3</sup> All calculations and simulations assume a 600 km,  $55^\circ$  inclination orbit, required to reach these high-energy particles. The attitude control system of CSSWE has two performance requirements:

1. The attitude control system shall have a settling time of less than 7 days.
2. Once settled, the CubeSat shall stay within  $\pm 15^\circ$  of the local magnetic field lines.

The ability to meet these requirements is entirely dependent on the PMAC system design; the requirements are

**Table 1. 3U CubeSat Environmental Torques\***

Torque	Value [N·m]
Aerodynamic	$8E - 8$
Gravity Gradient	$6E - 8$
Radiometric	$1E - 8$
RMS Sum	$1E - 7$

\*Assuming 600 km orbit

validated by a Matlab model. Figure 1 shows CSSWE with magnetic components highlighted in red.

There are two sources of error in effect when using a PMAC system. The first is steady state error, in which the hysteresis rod magnetic moment causes the total magnetic moment to be misaligned with the long axis of the spacecraft, decreasing pointing accuracy. Because the hysteresis rod polarity switches, this effect cannot be canceled using a particular hysteresis rod orientation. Steady state error becomes noticeable when the torque supplied by the bar magnet is on par with the hysteresis rod torque (when the angle between the CubeSat long axis and the local magnetic field is small). The second, oscillatory error, occurs because the magnetic field changes as the spacecraft travels, causing a delay before alignment with the current field.<sup>4</sup> The oscillatory error is directly related to the PMAC settling time, which may be of critical importance for a short mission duration. As hysteresis material is increased, the oscillatory error and settling time decrease at the cost of increased steady-state error, while decreasing the material has the opposite effect. A good PMAC system design will find the balance between these two errors when determining the hysteresis material needed for a given bar magnet strength.

### PMAC System Design

A successful attitude system design begins with an analysis of external torques experienced by the spacecraft. Table 1 shows the torques experienced by a 3U CubeSat at 600 km. The torque supplied by a magnetic moment in a magnetic field is quite simple:

$$\vec{T} = \vec{m} \times \vec{B}. \quad (1)$$

where  $\vec{B}$  is the magnetic flux density vector and  $\vec{m}$  is the magnetic moment vector for the bar magnet, though this equation is valid for the torque from a hysteresis rod magnetic moment as well. At 600 km,  $|\vec{B}|$  varies from 0.20 – 0.45 Gauss. The author presents a modified version of Santoni and Zelli’s recommended bar magnet

strength for the UNISAT-4 student satellite:<sup>5</sup>

$$m \geq 10 \frac{T_{RMS}}{B_{min} \cdot \sin(\beta_{max})} \quad (2)$$

where  $T_{RMS}$  is the root means squared sum of independent environmental torques,  $B_{min}$  is the minimum field strength at 600 km ( $2.0E - 5$  Tesla), and  $\beta_{max}$  is the desired pointing accuracy ( $10^\circ$ ).

### Bar Magnet Design

The bar magnet design is concerned with finding a suitable bar magnet magnetic moment. Equation 2 has been modified from Santoni and Zelli<sup>5</sup> to decrease the strength of the bar magnet, thus decreasing the required hysteresis material within the volume-limited CubeSat. This equation gives CSSWE the minimum  $m = 0.29$  A·m<sup>2</sup>.

A second constraint on the chosen bar magnet strength is parametric resonance, which can occur for polar orbits. The magnetic moments which resonate are given by the following system of equations:

$$\eta \cong 2.63k^2 - 0.49 + 0.51 \frac{I_{xx}}{I_{yy}} \quad (3)$$

$$\eta_{\perp} \cong 2.63k^2 - 4.25 + 1.25 \frac{I_{xx}}{I_{yy}} \quad (4)$$

$$m_{RES} = \frac{I_{yy} \cdot n_0^2 \cdot \eta}{B_{eq}} \quad (5)$$

$$m_{RES,\perp} = \frac{I_{yy} \cdot n_0^2 \cdot \eta_{\perp}}{B_{eq}} \quad (6)$$

where  $k$  is an integer,  $I_{xx}$  is the minor axis moment of inertia,  $I_{yy}$  is the major axis moment of inertia,  $n_0$  is the orbit mean motion, and  $B_{eq}$  is the magnetic flux density at the equator. Note Equations 5 and 6 are corrected from Santoni and Zelli.<sup>5</sup> For CSSWE and most CubeSats,  $I_{yy} \cong I_{zz}$ ;  $m_{RES}$  and  $m_{RES,\perp}$  should be recalculated for  $I_{zz}$  if  $I_{yy} \neq I_{zz}$ . Table 2 shows resonating magnetic moments for CSSWE surrounding the threshold set by Equation 2. This table assumes  $B_{eq} = 2.3E - 5$  Tesla,  $I_{xx} = 3.6E - 3$  kg·m<sup>2</sup>,  $I_{yy} = 1.7E - 2$  kg·m<sup>2</sup>, and 600 km orbit altitude. Considering the minimum value for  $m$  set by Equation 2 and the resonating values shown in Table 2, CSSWE has chosen  $m = 0.3$  A·m<sup>2</sup>.

### Hysteresis Rod Design

Once a bar magnet magnetic moment has been chosen, the hysteresis rod dimensions and quantity should be determined. Typically, hysteresis rods are mounted in pairs orthogonal to the bar magnet to maximize dampening per rod. Thus, we set the bar magnet in alignment with the long axis (X-axis) of the CubeSat, and place hysteresis rods in alignment with both short axes (Y and Z

**Table 2. CSSWE Parametric Resonances**

$k$	$\eta$	$\eta_{\perp}$	$m_{RES}$ [A·m <sup>2</sup> ]	$m_{RES,\perp}$ [A·m <sup>2</sup> ]
10	262.62	259.01	0.228	0.225
11	317.85	314.24	0.277	0.273
12	378.34	374.73	0.329	0.326
13	444.09	440.48	0.386	0.383
14	515.10	511.49	0.448	0.445
15	591.37	587.76	0.514	0.511

axes). The rods supply dampening by shifting polarities in delayed response to the magnetic field changes, converting rotational energy into heat. A hysteresis loop describes the rod's induced magnetic flux density for a given magnetic field strength, and is generally characterized by three magnetic hysteresis parameters: the coercive force  $H_c$ , the remanence  $B_r$ , and the saturation induction  $B_s$ , shown in Figure 2. These parameters are important in describing the shape of the hysteresis loop, the area of which determines the dampening per cycle per unit volume. However, the magnetic parameters vary with rod length to diameter  $L/D$  ratio, material, and external field strength. The dimensions and number of rods are set in response to the estimated magnetic hysteresis parameters.

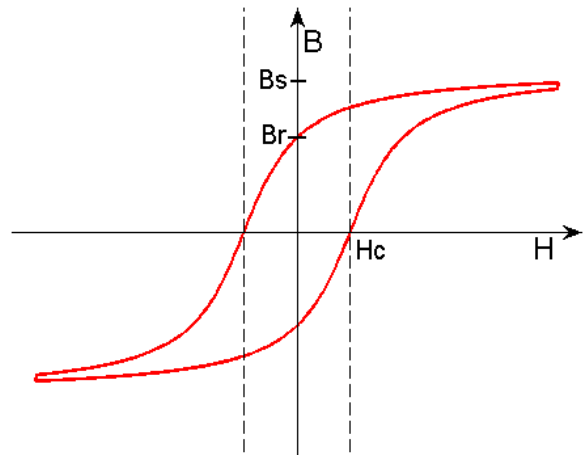
There are a number of ways to estimate the magnetic hysteresis parameters: Levesque uses true permeability rated material numbers regardless of rod dimensions,<sup>4</sup> Santoni and Zelli estimate the apparent permeability of the rod based on dimensions and applied field parameter values,<sup>5</sup> while Flatley and Henretty use empirically-determined values for a specific rod.<sup>6</sup> While empirical calculations are ideal, the design of a testing apparatus is beyond the scope of this paper. Instead, the author outlines a process to estimate the apparent hysteresis rod parameters. To begin, the magnetic moment supplied by a hysteresis rod is given by:

$$m_{hyst} = \frac{B_{hyst} \cdot V_{hyst}}{\mu_0} \quad (7)$$

where  $m_{hyst}$  is the magnetic moment of the hysteresis rod aligned with its long axis,  $B_{hyst}$  is the magnetic flux induced in the rod,  $V_{hyst}$  is the volume of the rod, and  $\mu_0$  is the permeability of free space.<sup>6</sup> The induced magnetic flux is broken down to:

$$B_{hyst} = \mu_0 \mu'_{hyst} H \quad (8)$$

where  $H$  is the magnetic field strength and  $\mu'_{hyst}$  is the apparent relative permeability of the rod. Because the hysteresis rod is ferromagnetic material,  $\mu'_{hyst}$  varies

**Figure 2. Hysteresis loop diagram**

with  $H$  and  $B_{hyst}$  and is non-linear,<sup>5</sup> as shown in Figure 2. The apparent permeability may be defined as:

$$\mu'_{hyst} = \frac{\mu_{hyst}(H)}{1 + N\mu_{hyst}(H)} \quad (9)$$

where  $N$  is the demagnetizing factor of the rod and  $\mu_{hyst}$  is the true relative permeability of the rod which varies with  $H$ .<sup>5</sup> Note that  $\mu_{hyst}$  is always greater than  $\mu'_{hyst}$ , and the discrepancy between the two grows with  $N$ . The demagnetization factor for the long axis of a cylinder is given by:<sup>7</sup>

$$N = \left[ \left( \frac{L}{D} \right) \frac{4}{\sqrt{\pi}} + 2 \right]^{-1} \quad (10)$$

Clearly, the hysteresis rod  $L/D$  ratio affects the value of  $N$ , and thus the efficiency of the rod. We combine Equations 8 - 10 to estimate the expected hysteresis rod apparent saturation induction:

$$B'_s = \mu_0 \mu'_{hyst} H_s = \mu_0 \left( \frac{\mu_{hyst}(H_s)}{1 + \mu_{hyst}(H_s) \left( \left( \frac{L}{D} \right) \frac{4}{\sqrt{\pi}} + 2 \right)^{-1}} \right) H_s \quad (11)$$

where  $H_s$  is the magnetic field strength at saturation ( $H$  when  $B = B_s$ ). Typical values of  $L/D$  are  $\sim 100 - 300$ ,<sup>1</sup> and CubeSat interior dimensions set an upper limit so  $L \leq 9.5$  cm. Recognizing this, we use  $L/D = 95$  and find  $D = 1$  mm (for ease of manufacturing). The chosen hysteresis rod material (HyMu-80) has a material saturation field strength  $H_s = 100$  A/m.<sup>5</sup> Using this  $H_s$  and Figure 3, we find  $\mu_{hyst}(H_s) = 1.5E + 4$ . Using Equation 11 with these values estimates  $B'_s = 0.0268$  Tesla. However,  $H'_c$  and  $B'_r$  cannot be calculated the same way, so we instead estimate their values equivalent to those

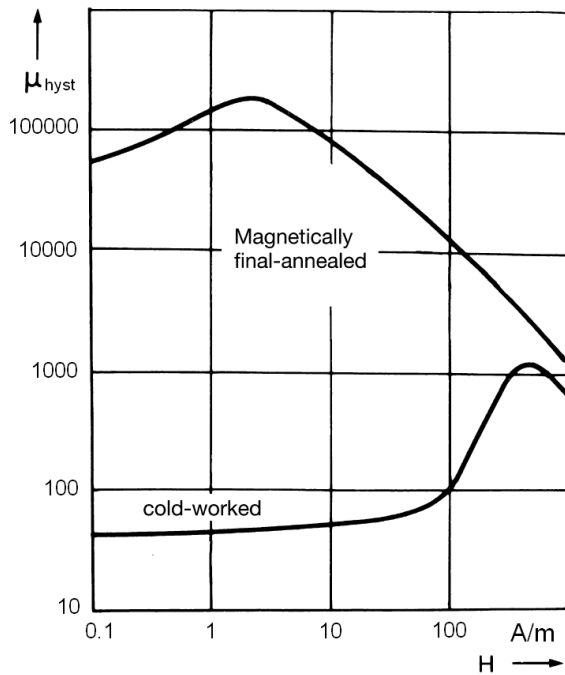


Figure 3. Hysteresis rod true permeability<sup>8</sup>

Table 3. Hysteresis Rod Comparison

Property	UNISAT-4 <sup>5</sup>	CSSWE
Rod Length [cm]	15	9.5
Rod Diameter [mm]	1	1
Material	HyMu-80	HyMu-80
Material $H_c$ [A/m] <sup>8</sup>	0.96	0.96
Material $B_r$ [Tesla] <sup>4</sup>	0.35	0.35
Material $B_s$ [Tesla] <sup>8</sup>	0.74	0.74
Apparent $H'_c$ [A/m]	12	12*
Apparent $B'_r$ [Tesla]	0.004	0.004*
Apparent $B'_s$ [Tesla]	0.025	0.027**

\*Estimated value

\*\*Calculated value

empirically derived from a similar rod.<sup>5</sup> This assumption is valid because the calculated  $H'_s$  is very close to the UNISAT-4 value. Table 3 compares the hysteresis rod properties of UNISAT-4 and CSSWE. Note that the values of  $H_c$  and  $B_r$  are estimated values and should be empirically tested before completing the design of a PMAC system. Now that the physical properties of each rod have now been estimated, an attitude simulation is developed to determine the number of rods per axis needed to satisfy the pointing requirements.

## Matlab Attitude Simulation

The attitude simulation begins with a choice of attitude coordinates. The author has chosen 3-2-1 Euler angles; this attitude coordinate set results in the following kinematic differential equation of motion:

$$\begin{pmatrix} \dot{\theta}_1 \\ \dot{\theta}_2 \\ \dot{\theta}_3 \end{pmatrix} = \frac{1}{c\theta_2} \begin{bmatrix} 0 & s\theta_3 & c\theta_3 \\ 0 & c\theta_3 c\theta_2 & -s\theta_3 c\theta_2 \\ c\theta_2 & s\theta_3 s\theta_2 & c\theta_3 s\theta_2 \end{bmatrix} \begin{pmatrix} \omega_x \\ \omega_y \\ \omega_z \end{pmatrix} \quad (12)$$

where  $\theta_1, \theta_2, \theta_3$  are the Euler angles,  $\dot{\theta}_1, \dot{\theta}_2, \dot{\theta}_3$  are the Euler angle rates and  $\omega_x, \omega_y, \omega_z$  are the body-fixed angular velocities of the X Y Z axes respectively. Also note that  $c\theta$  is  $\cos \theta$  and  $s\theta$  is  $\sin \theta$ . Now we assume a body frame aligned with the principal axes of the CubeSat (constant diagonal mass matrix) and use Euler's separated rotational equations of motion to complete the equation set:

$$I_{xx}\dot{\omega}_x = -(I_{zz} - I_{yy})\omega_y\omega_z + L_x \quad (13)$$

$$I_{yy}\dot{\omega}_y = -(I_{xx} - I_{zz})\omega_z\omega_x + L_y \quad (14)$$

$$I_{zz}\dot{\omega}_z = -(I_{yy} - I_{xx})\omega_x\omega_y + L_z \quad (15)$$

where  $I_{xx}, I_{yy}, I_{zz}$  are the mass moment of inertias of the principal axes which align with the body fixed X Y Z axes respectively,  $\dot{\omega}_x, \dot{\omega}_y, \dot{\omega}_z$  are the body fixed angular accelerations for the X Y Z axes respectively, and  $L_x, L_y, L_z$  are the external torques on the X Y Z axes respectively.<sup>9</sup> With the equations of motion defined, we investigate the external torques acting on the CubeSat.

### External Torque: Bar Magnet

While the bar magnet torque is simply given by Equation 1, the value of  $\vec{B}$  varies with both orbit location, and the current attitude configuration. Keep in mind that  $\vec{B}$  is the magnetic field experienced by the bar magnet and must be examined in a body-fixed frame. The simulation has two frames: body-fixed and the Earth Centered Earth Fixed (ECEF) inertial frame. The Direction Cosine Matrix (DCM) which allows rotation from inertial to body-fixed frame for 3-2-1 Euler angles is given below:

$$\begin{bmatrix} c\theta_2 c\theta_1 & c\theta_2 s\theta_1 & -s\theta_2 \\ s\theta_3 s\theta_2 c\theta_1 - c\theta_3 s\theta_1 & s\theta_3 s\theta_2 s\theta_1 + c\theta_3 c\theta_1 & s\theta_3 c\theta_2 \\ c\theta_3 s\theta_2 c\theta_1 + s\theta_3 s\theta_1 & c\theta_3 s\theta_2 s\theta_1 - s\theta_3 c\theta_1 & c\theta_3 c\theta_2 \end{bmatrix} \quad (16)$$

The DCM is defined as

$\{\hat{\mathbf{b}}\} = [C(\theta_1, \theta_2, \theta_3)]\{\hat{\mathbf{n}}\}$  where  $\{\hat{\mathbf{b}}\}$  is the body-frame vector,  $[C(\theta_1, \theta_2, \theta_3)]$  is the DCM, and  $\{\hat{\mathbf{n}}\}$  is the inertial frame vector.<sup>9</sup> We now have the tools to use a model of the Earth's magnetic field strength in the simulation. Rauschenbakh et al. define the following dipole model

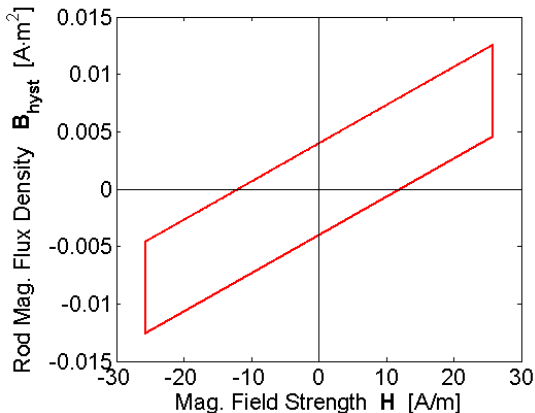


Figure 4. Modeled Apparent Hysteresis Loop

in ECEF frame:

$$H_1 = 3H_{eq} \sin i \cos i \sin^2 u \quad (17)$$

$$H_2 = -3H_{eq} \sin i \sin u \cos u \quad (18)$$

$$H_3 = H_{eq}(1 - 3 \sin^2 i \sin^2 u) \quad (19)$$

where  $H_{eq}$  is the equatorial magnetic field strength magnitude at 600 km (18.3 A/m),  $i$  is the orbit inclination ( $55^\circ$ ),  $u$  is the argument of latitude, and  $H_1, H_2, H_3$  is the magnetic field strength in the ECEF direction vectors 1,2,3 respectively.<sup>10</sup> An argument of latitude value is linked to each timestep, simulating the CubeSat motion through each orbit. At each timestep the DCM is used to determine the magnetic field seen by the CubeSat, which is then used to determine the external torque due to the bar magnet.

#### External Torque: Hysteresis Rods

Simulating the hysteresis response begins by developing a hysteresis loop model. Flatley and Henretty develop the following model:<sup>6</sup>

$$p = \frac{1}{H_c} \tan \left( \frac{\pi B_r}{2B_s} \right) \quad (20)$$

$$B_{hyst} = \frac{2}{\pi} B_s \tan^{-1} [p(H \pm H_c)] \quad (21)$$

where  $p$  is a constant for a given set of magnetic hysteresis parameters and  $H$  is the component of the magnetic field strength aligned with the hysteresis rod. Notice the  $\pm H_c$  term of Equation 21. A value of  $+H_c$  is used when  $dH/dt < 0$  and  $-H_c$  is used when  $dH/dt > 0$ . This term is essential in defining the delay of the hysteresis loop, though it does create a headache when coding the model in an ODE solver such as Matlab's ode45. Because the angular position of the rod defines the component of the magnetic field aligned with the rod, the previous value of

$H$  as seen by the rod must be available at each timestep to define  $dH/dt$ . However, the previous time need not be saved as only the threshold of  $dH/dt$  above or below zero matters for this model.

This model ensures that  $H_c$  and  $B_r$  cross the X and Y axes as shown in Figure 2. The material hysteresis parameters in Equations 20 and 21 may be interchanged for the apparent hysteresis parameters to simulate non-ideal, realistic rods. Figure 4 shows the hysteresis loop generated by using the apparent parameters in Table 3 with the models for Earth magnetic field and hysteresis developed thus far. The hysteresis loop is cut off because the maximum variation of the Earth magnetic field strength component is  $\pm 25.8$  A/m at 600 km; the Earth magnetic forcing is not large enough to induce  $B'_s$ . Note an ideal assumption associated with this model: we use only one hysteresis loop to model the hysteresis response. In reality, a different hysteresis loop is generated for each field strength cycle range. If empirical data for various field strength loops are available, the hysteresis response for multiple field strength ranges may be simulated.<sup>6</sup>

#### Matlab ODE Solver Pitfalls

Through a series of unfortunate events, the author has discovered a few pitfalls associated with built-in Matlab ODE numerical solvers. The first of these pitfalls is to assume the absolute and relative tolerances may be set to default values  $1E-6$  and  $1E-3$  respectively. To test this, we developed a simplified two-dimensional model to simulate the basic dynamics, using the Hysteresis Model shown above to simulate one hysteresis rod in a constant magnetic field. This model was given an initial rotation rate and run using Matlab's ode45 numeric integrator. Figure 5 shows the behavior of the model for varying values of relative and absolute tolerance. The dynamic response for each Matlab ODE solver converges at a tolerance of  $1E-7$ ; this value is used for all subsequent Matlab ODE solver inputs.

The second pitfall is to assume all Matlab solvers behave equally. Figure 6 shows the results from the same two-dimensional model, this time run with different Matlab ODE solvers (tolerance:  $1E-7$ ). The results show that the slope of the angular velocity envelope, directly correlated with the settling time of the simulation, varies by solver. However, the author has chosen to use the ode45 solver due to its known robustness.

## Simulation Results

The input assumptions for the Matlab PMAC simulation are shown in Tables 3 (apparent values) and 4. The first model run simulates one hysteresis rod on the Y and Z axes. The angular velocity decay over time is shown in

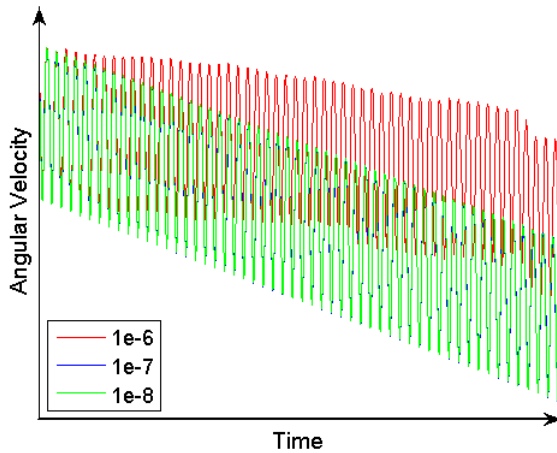


Figure 5. Matlab Tolerance Effect

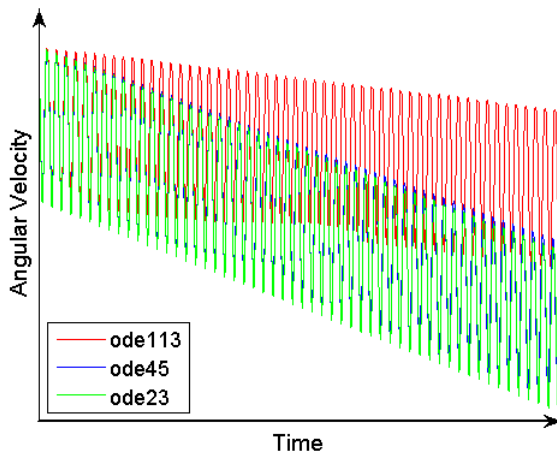


Figure 6. Matlab Solver Effect

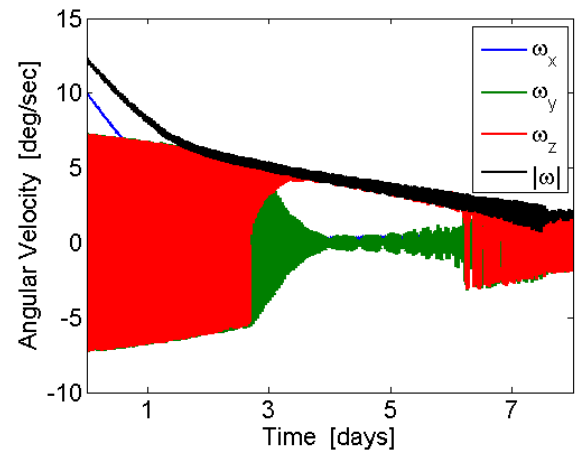


Figure 7. Angular Velocity, 1 Rod / Axis

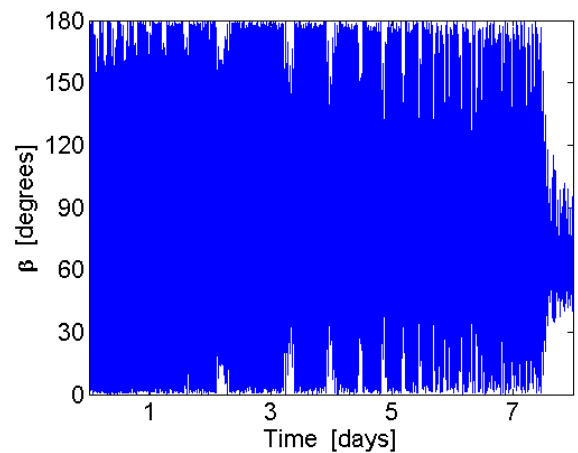


Figure 8. Beta, 1 Rod / Axis

Table 4. CSSWE Input Assumptions

Input	Value
Rods per axis Y Z	2
$(\theta_{10}, \theta_{20}, \theta_{30})$ , [°]	(0,0,0)
$(\omega_{x0}, \omega_{y0}, \omega_{z0})$ , [°/sec]	(10,5,5)
$I_{xx}$ [kg·m <sup>2</sup> ]	0.00551
$I_{yy}$ [kg·m <sup>2</sup> ]	0.02552
$I_{zz}$ [kg·m <sup>2</sup> ]	0.02565
Relative Tolerance	1E - 7
Absolute Tolerance	1E - 7

Figure 7. Figure 8 shows the angle  $\beta$ , the angle between the CubeSat long axis and the local magnetic field, vs. time. Clearly, there is not enough dampening material to meet the required 7 day settling time. Next, the simulation is run adding another rod on the Y and Z axes. The angular velocity decay with two rods per axis is shown in Figure 9. Figure 10 shows that the settling time requirement of 7 days is met, while the zoomed 11 shows  $\beta$  within the  $\pm 15^\circ$  requirement. However, Figure 11 must be viewed with equation 2 in mind. Because the PMAC system was designed for  $\beta_{max} = 10^\circ$ , at  $\beta < 10^\circ$ , the magnetic torques enter the domain of the environmental torques shown in Table 1, where they will disturb the attitude of the CubeSat. The total estimated mass of the 4 hysteresis rods<sup>8</sup> + bar magnet is 8.6 grams (not including mounting structure).

## Conclusion

We describe the Passive Magnetic Attitude Control (PMAC) system for the Colorado Student Space Weather Experiment (CSSWE) CubeSat. PMAC is a wise choice for the mission due to its ability to align the CubeSat within  $\pm 15^\circ$  of the Earth's magnetic field at a cost of 8.6 grams and no power. This aligns the science instrument for a maximized signal. The design is completed by first considering the bar magnet strength, then setting a hysteresis volume in response. After considering the environmental torques on the CubeSat and the possibility of parametric resonance, the magnetic moment of the bar magnet is chosen at  $0.3 \text{ A}\cdot\text{m}^2$ . Next, the hysteresis response is considered by estimating the parameters which define the material hysteresis loop for specific rod dimensions and magnetic field strength. The chosen hysteresis rod dimensions are 1mm diameter  $\times$  9.5 cm length.

The attitude simulation is described in terms of the chosen 3-2-1 Euler angle attitude coordinates and the kinematic differential equations of motion. The Euler rotational equations of motion complete the differential equation set needed to simulate the CubeSat attitude. Next, the external torques inputs of these equations are considered. The bar magnet external torque is defined by both the orientation of the spacecraft and a chosen dipole model of Earth's magnetic field. The hysteresis rod torque is dependent on the previous and current time step magnetic fields, which are used to determine the induced magnetism in the rod. With the simulation fully described, two pitfalls of Matlab ODE solvers are discussed: choice of absolute and relative tolerance ( $1\text{E-}7$ ), and choice of ODE solver (ode45).

Next, the simulation results are presented. One rod per axis is dismissed because it does not meet the set PMAC requirements. Two rods per axis are chosen based on the model results, which show that the CSSWE PMAC is sufficient to bring the CubeSat to within  $\pm 10^\circ$  of the local magnetic field lines. Although the CSSWE design is outlined, this paper can be used to design the PMAC system for any spacecraft. PMAC is useful when the mission is benefited by loose alignment with the local magnetic field and mission budgets are tight. As shown, the dynamics can be sufficiently simulated to validate the design of a PMAC system.

## Acknowledgements

The author first and foremost thanks the CSSWE team, current and previous. It is their effort and enthusiasm lifting the CubeSat off the ground each day. I am also grateful to Dr. Scott Palo and Dr. Xinlin Li, who have provided invaluable support for the past

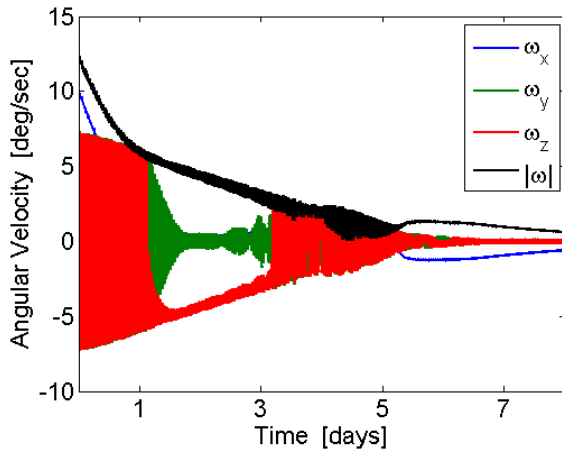


Figure 9. Angular Velocity, 2 Rod / Axis

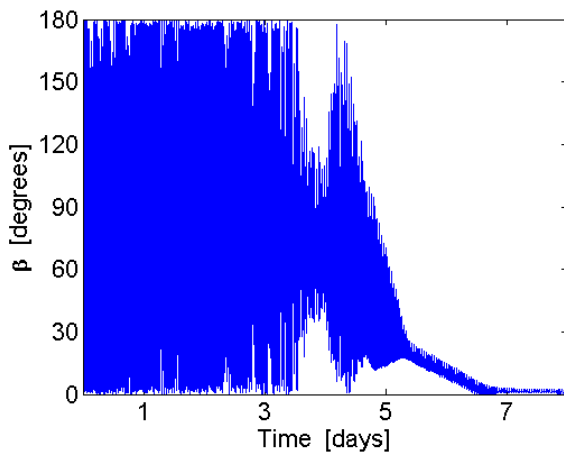


Figure 10. Beta, 2 Rod / Axis

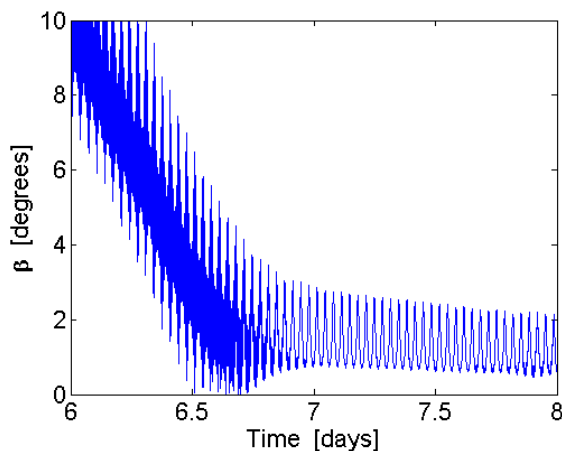


Figure 11. Beta, 2 Rod / Axis, Zoomed

two years. The National Science Foundation funding has made space hardware development a reality for this grad student and others. Laboratory for Atmospheric and Space Physics engineers Rick Kohnert, Vaughn Hoxie, and Susan Batiste have provided support for CSSWE since the inception of the project, and continue to do so today. Dr. H.P. Schaub literally taught the author everything he knows about attitude dynamics. Finally, the author thanks Joe Tanner for supporting graduate projects at the University of Colorado.

### References

<sup>1</sup>Ovchinnikov, M. Y. and Penkov, V., “Passive Magnetic Attitude Control System for the Munin Nanosatellite,” *Cosmic Research*, Vol. 40, No. 2, 2002, pp. 142–156.

<sup>2</sup>University of Michigan, *In-Lab Testing for Attitude Determination and Control*, Logan, UT, 2009, CubeSat Workshop.

<sup>3</sup>Schiller, Q. and Mahendrakumar, A., “REPTile: a miniaturized detector for a CubeSat mission to make valuable measurements of relativistic particles in near-Earth space,” *Small Satellite Conference*, AIAA/USU, 2010.

<sup>4</sup>Levesque, J.-F., “Passive Magnetic Attitude Stabilization using Hysteresis Materials,” Tech. Rep. SIGMA-PU-006-UdeS, Université de Sherbrooke, 1995.

<sup>5</sup>Santoni, F. and Zelli, M., “Passive Magnetic Attitude Stabilization of the UNISAT-4 microsatellite,” *Acta Astronautica*, Vol. 65, 2009, pp. 792–803.

<sup>6</sup>Flatley, T. W. and Henretty, D. A., “A Magnetic Hysteresis Model,” Tech. Rep. N95-27801, NASA GSFC, 1995.

<sup>7</sup>Sato, M. and Ishii, Y., “Simple and approximate expressions of demagnetizing factors of uniformly magnetized rectangular rod and cylinder,” *Journal of Applied Physics*, Vol. 66, No. 2, 1989, pp. 983–985.

<sup>8</sup>Vacuumschmelze, *Soft Magnetic Materials and Semi-finished Products*, pht-001 ed., 2002.

<sup>9</sup>Schaub, H. and Junkins, J. L., *Analytical Mechanics of Space Systems*, American Institute of Aeronautics and Astronautics, Inc., 1st ed., 2003.

<sup>10</sup>Rauschenbakh, B. V., Ovchinnikov, M. Y., and McKenna-Lawlor, S., *Essential Spaceflight Dynamics and Magnetospherics*, chap. SC Motion in the Geomagnetic Field, Microcosm Press and Kluwer Academic Publishers, 2004.